A&A 459, 777–781 (2006)
DOI: 10.1051/0004-6361:20065959

Astronomy & Astrophysics

A search for stellar X-ray sources in the Sagittarius and Carina dwarf galaxies

I. X-ray observations⋆

G. Ramsay[1] and K. Wu[1,2]

[1] Mullard Space Science Laboratory, University College London, Holmbury St. Mary, Dorking, Surrey, RH5 6NT, UK
e-mail: gtbr@mssl.ucl.ac.uk
[2] School of Physics A28, University of Sydney, NSW 2006, Australia

Received 3 July 2006 / Accepted 26 August 2006

ABSTRACT

ROSAT observations found no convincing evidence for X-ray sources located in local dwarf spheroidal galaxies (dSph). Now with more sensitive instruments on board *Chandra* and *XMM-Newton* we can reach fainter luminosity levels. We report on an observation of the Sagittarius (Sgr) dSph made using *Chandra* and an observation of the Carina (Car) dSph made using *XMM-Newton*. Our observations are sensitive to sources with X-ray luminosities in the 0.1–10 keV band of $\sim 1 \times 10^{32}$ erg s^{-1} and $3{\times}10^{34}$ erg s^{-1} for the Sgr and Car fields respectively. We have identified a total of 80 sources in the Sgr field and 53 sources in the Car field. Although the source numbers are roughly consistent with the expected number of background AGN, we found a small fraction of X-ray sources which were soft and could be located in the host dSph. Follow-up optical/IR observations may help to identify their optical counterparts and hence determine their nature.

Key words. galaxies: dwarf – galaxies: individual: Sagittarius – galaxies: individual: Carina – X-rays: binaries – X-rays: galaxies

1. Introduction

Dwarf galaxies are low luminosity galaxies and make up a large fraction of galaxies at the present epoch (Marzke & da Costa 1997). Because of their faintness, the best studied systems reside in the Local Group. The Milky Way has 12 known satellite galaxies. With the exception of the LMC and SMC, which are irregulars, all of them are dwarf spheroidals (dSphs). DSphs are generally gas poor and have low metallicity. Their star formation activity has long since ceased, and their stellar populations are old. (See Mateo 1998 for a review of Local Group dwarfs.)

While the Local Group dSphs have been well studied in the optical and infra-red, their X-ray properties are yet to be established. DSphs were seldom observed in the X-ray band, in the belief that they do not contain substantial number of detectable X-ray sources. A *ROSAT* observation of the Fornax dSph (which is at a distance of 138 kpc) found 19 sources in the field (Gizis et al. 1993). Since this number was consistent with the expected number of background AGN, the sources were not thought to be stellar binary sources located in the dSph. A recent *Chandra* observation of the Sculptor dSph (at a distance of 79 kpc) identified 5 sources which were likely to be located in that galaxy (Maccarone et al. 2005). They have inferred X-ray luminosities $L_{\rm x} \sim 6$–90×10^{33} erg s^{-1}, which are well below 10^{37}–10^{38} erg s^{-1}, typical luminosities of bright Galactic X-ray binaries. From these studies we may conclude that dSphs in the Local Group do not have a significant number of bright X-ray sources (see Zang & Meurs 2001).

The number of binary X-ray sources in a galaxy is determined by the formation rate of the sources and the rate at which the sources cease to be X-ray active. Also, it depends on the duration of the X-ray duty cycles of the sources. Observations show that X-ray sources are more abundant in starburst galaxies and interacting galaxies than in the "milder" galaxies (see e.g. Fabbiano 2003), and the brightness distribution of X-ray sources vary with their host environments even within the same galaxy. For instance in spiral galaxies, e.g. M81 (Tennant et al. 2001; Swartz et al. 2003), sources in the galactic disks have power-law luminosity functions, while sources in galaxy bulges tend to have broken power-law like or exponential cut-off type luminosity functions. Now there is strong evidence that X-ray source populations in galaxies and their brightness distribution are dependent on the star formation activity of the source host environment in recent epochs. This phenomenon can be explained by a birth-death process as that described in Wu (2001). The lack of very bright sources in old stellar populations can be explained by the fact that X-ray sources have finite life-spans and bright sources which require rapid mass transfer are short-lived. If the mass transfer rate in a binary is sufficiently low or if the mass-transfer active phase in its duty cycle is sufficiently short, the system may survive a very long time as an X-ray source. The source may exhibit alternating active and faint states, and so it may not be easily identified in a single snap-shot observation.

In the birth-death model presented in Wu (2001), there is also an old X-ray source population in any galaxy whose progenitors were the first-generation stars formed in the very early epoch. These "primordial" binary X-ray sources are dim, and their mass-donor stars are low-mass stars. As these binaries have a sustainable mass-transfer phase spanning over a period

⋆ Appendix A is only available in electronic form at http://www.aanda.org

of >10 Gyr, the average mass-transfer rate between cannot exceed 10^{15} g s^{-1}. If the accreting compact object is a black hole or a neutron star, the X-ray luminosity of the binary would be $<10^{35}$ erg s^{-1}. Even when a detection limit of well below 10^{35} erg s^{-1} has been achieved, the old binary X-ray sources are not easily identified in big spiral galaxies like M31 or M81 (see e.g. Kong et al. 2003; Swartz et al. 2003), because there are hundreds of younger X-ray sources with luminosities above 10^{36} erg s^{-1}. DSphs have not had recent star formation activity and are therefore the most appropriate targets to search for the old X-ray source population.

ROSAT had the sensitivity to detect sources brighter than $\sim 10^{34}$ erg s^{-1} in the nearby dSphs but were unable to detect sources with luminosities of 10^{32} erg s^{-1}. With *Chandra* and *XMM-Newton*, we can now search for sources with luminosities below 10^{32} erg s^{-1} in the dwarf satellites of the Milky Way. We have made X-ray observations of the Sagittarius dSph (Sgr) with *Chandra* in 2003 and Carina dSph (Car) with *XMM-Newton* in 2004. This paper presents the results of our X-ray observations of these two galaxies. (The *Chandra* observation of Sgr was centered near the globular cluster M 54, and analysis of the cluster sources has already been presented in Ramsay & Wu (2006).)

Sgr, at a distance of 27.4 kpc (Layden & Sarajedini 2000), is the second closest satellite to the Milky Way. It extends over at least $22^\circ \times 8^\circ$ in the sky, and is located on the far side of the Milky Way to the Sun (Ibata et al. 1994, 1995). The absorption column density along the line-of-sight is relatively high (1.2×10^{21} cm^{-2}) because of the low galactic latitude of Sgr (-14°), Star formation in Sgr mostly ceased $\sim$10 Gyr ago (Mateo 1998). Car was discovered in plates taken using the UK Schmidt Telescope (Cannon et al. 1977) and is 100 kpc distant (van den Bergh 2000). The line-of-sight absorption column to Car is 3.9×10^{20} cm^{-2}. Car has had a more complex star formation history than Sgr: around half of its stars were formed 7 Gyr ago, the remainder occuring at 15 and 3 Gyr ago (Hurley-Keller et al. 1998).

2. Observations and data analysis

2.1. Sagittarius dwarf galaxy

Sgr was observed with *Chandra* ACIS-I for 30 ksec on 2003 Sep. 3. The total field of view was $16.9' \times 16.9'$. The pointing was centered on $\alpha_{2000} = 18^{\rm h}55^{\rm m}3.0^{\rm s}$, $\delta_{2000} = -30^\circ 28' 59''$: this was offset from the center of the globular cluster M 54 by $-12''$ in declination. Front illuminated CCDs 0–3 were used. The "read" mode was configured in `TIMING` mode; the "data" mode was `VERY FAINT`. During the observation the solar particle background was very low.

We used the primary data products as supplied by the *Chandra* Data Archive Operations. A source search was initially performed on each CCD separately in the 0.3–8.0 keV band using `wavedetect` in the CIAO v3.0 software package. This was done in conjunction with an exposure map using a mean photon energy of 1.5 keV. We rejected all "sources" with fewer than 5 counts (not background subtracted) in the 0.3–8 keV band. The resulting source list was then compared by-eye with the image in that band: "sources" which were not clear in the image were not counted. We detected a total of 80 sources, excluding the 7 sources belonging to the globular cluster M 54 (Ramsay & Wu 2006). Assuming a power law spectral model with a spectral index of 1.4 and an absorption column of 1.2×10^{21} cm^{-2}, we obtain a sensitivity level of 4.0×10^{-15} erg cm^{-2} s^{-1} (unabsorbed flux) in the 0.3–8 keV band. The inferred unabsorbed flux in the 0.1–10 keV band is 4.6×10^{-15} erg cm^{-2} s^{-1}, corresponding to a luminosity of 1.1×10^{32} erg s^{-1} for the distance to Sgr.

Using the source list derived above, we also determined the counts for each source in the 0.3–1 keV (S), 1–2 keV (M) and 2–8 keV (H) bands (which will be used to construct the colour-colour plots following the convention considered in Prestwich et al. (2003), Soria & Wu (2003) and Swartz et al. (2004)). To determine the mean background count rate in each band we created an event file which excluded the detected sources. We then scaled the number of events in the sampled area with the mean size of the extraction region. In the 2–8 keV band a total of 45 sources are detected above the 2.0-σ level. We show the list of sources with their counts in each band in the Appendix.

2.2. Carina dwarf galaxy

Car was observed by *XMM-Newton* on 2005 May 25 for 41.7 ksec. Both the EPIC MOS (Turner et al. 2001) and the EPIC pn (Strüder et al. 2001) wide field instruments were in full frame mode and used thin filters. The diameter of the EPIC MOS field is approximately 28′, and the field of view of the EPIC pn is approximately $27' \times 27'$. The field center was $\alpha_{2000} = 6^{\rm h}41^{\rm m}37^{\rm s}$, $\delta_{2000} = -50^\circ 58' 0''$. The data were analysed using the *Science Analysis Software* (SAS) v6.0.

The calibrated MOS1 and MOS2 event data were combined and analysed separately from the EPIC pn data. Data from the first 400 s were excluded from the analysis since the background was significantly higher than the following data. Events which had `PATTERN=0-12` and `FLAG=0` were used. Images and exposure maps were extracted.

These data were searched for sources with the resulting source list being examined by eye – "sources" which were not visible as such in the 0.2–10 keV images were removed from the source list. Some sources were only detected in the MOS instruments because they were located in the pn chip gaps (and vice versa). A total of 53 sources were detected. Their count rates were determined in the energy ranges: 0.2–1 keV, 1–2 keV and 2–10 keV. In the 2–10 keV band 41 sources were detected above 2.0-σ level. The source positions, count rates and X-ray colours are given in the Appendix.

Assuming a power law spectral model with a spectral index of 1.4 and an absorption column of 3.9×10^{20} cm^{-2}, we obtain a flux sensitivity level of 2.8×10^{-14} erg cm^{-2} s^{-1} in the 0.2–10 keV band (unabsorbed). This corresponds to an unabsorbed flux of 2.9×10^{-14} erg cm^{-2} s^{-1} in the 0.1 − 10 keV band, and a luminosity of 2.9×10^{34} erg s^{-1} for the distance to Car.

3. Source brightness distributions

Figure 1 shows the cumulative luminosity function, $N(>S)$ (where S is the count rate), of the Sgr and Car sources. The luminosity function of the Sgr sources in the 0.3–8 keV band shows a flattening at its faint end where the count rate falls below $\sim 2.3 \times 10^{-4}$ ct s^{-1}. The flattening is not seen in the luminosity function for the 2–8 keV band. The luminosity functions of the Car sources in the 0.2–10 keV and 2–10 keV bands appear similar and have no obvious features. The flattening in the luminosity function of Sgr sources at the 0.3–8 keV band is probably not due to the change in the distribution of the intrinsic brightness of the sources but incompleteness caused by high absorption at energies below 1 keV in the direction to galaxy.

We used the Bayesian algorithm, derived by Wheatland (2004), to determine the slope of the luminosity function and

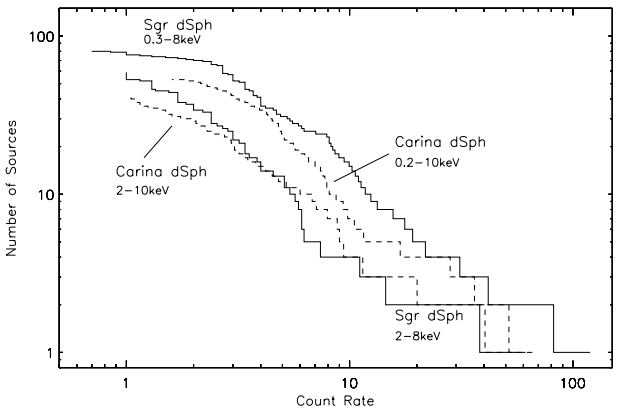

Fig. 1. The cumulative luminosity functions ($N(>S)$ as a function of count rate S) of the sources in the Sgr and Car fields in 2 energy bands. The count rate for the Sgr sources is ct/10 ks and ct/ks for the Car sources.

obtained a power-law index $\alpha = 1.42 \pm 0.16$ for the Sgr sources with a cut-off at 2.3 counts/10 ks at the 0.3–8 keV band. The slope is slightly steeper than that for the sources in the globular cluster M 54 (0.90 ± 0.34, Ramsay & Wu 2006). For the luminosity function of the Car sources in the 0.2–10 keV band we obtained a power-law slope of $\alpha = 1.39 \pm 0.05$. At the 2–8 keV band the slope of the Sgr sources (1.03 ± 0.13) is flatter than that of the Car sources (1.36 ± 0.06). They are steeper than the slope of the sources (0.61 ± 0.10) in the *Chandra* north and south deep fields in the 2–10 keV band (Rosati et al. 2002). However, they are similar to the slope in the 5–10 keV band (1.35 ± 0.15).

To determine if any of the sources were bright foreground stars we correlated our X-ray positions with the UCAC2 catalogue (Zacharias 2004). This catalogue is complete down to $R = 16$ and has astrometry better than 70 milli-arcsec. For the Sgr field we found 5 X-ray sources which had optical counterparts within a 2 arcsec radius, while for Car, we found 6 sources within a 4 arcsec radius (the error circle for the *XMM-Newton* positions were greater than for *Chandra*). The UCAC2 mag for these sources is given in Tables A.1–A.2. We classify these sources as likely foreground objects.

We estimated the expected number of background AGN in the field of view using the luminosity function of the *Chandra* Deep Field South (CDF-S) sources. We considered the 2–10 keV band in which the effect of extinction is reduced. Assuming a power-law spectral model with a spectral index of 1.4 and an absorption column density to the edge of our galaxy in the line-of-sight, the sensitivity limit in the 2–10 keV band is 3.7×10^{-15} erg cm^{-2} s^{-1} for the Sgr sources and 1.9×10^{-14} erg cm^{-2} s^{-1} for the Car sources. The number of background AGN in the Sgr field would be about 55–79 and the number in the Car field about 16–34. The number of Sgr sources in the 2–8 keV band is 42 (after the subtraction of 3 sources which are likely foreground objects), which is slightly below the expected number if background AGN. The number of identified sources in the 2–10 keV band in the Car field is 40 (after the subraction of 1 source which was a likely foreground object), which is slightly above the expected number of background AGN. Whilst it is likely that the majority of the sources in the fields are background AGN, we cannot rule out at this stage the possibility that a few of the sources are stellar binary sources belonging to the two dSphs.

4. Luminosity estimates

In Sect. 3 we estimated the sensitivity limits in various energy bands assuming a power law spectral model of slope 1.4. We also estimated the count to flux conversions assuming a power-law spectral model with slope of 1.7 and with a blackbody model with $kT_{\rm bb} = 0.1$ keV and found that making an assumption of one conversion factor for all spectra – irrespective of their colour – in general gives an uncertainty of 30% in the source luminosity.

4.1. Sagittarius dwarf galaxy

We applied a conversion in which 10^{-4} ct s^{-1} in the 0.3–8 keV band is equivalent to an unabsorbed flux of 1.8×10^{-15} erg cm^{-2} s^{-1} in the 0.1–10 keV band. For this conversion, the inferred luminosities of the Sgr sources would be $\sim 1 \times 10^{32}$–2×10^{34} erg s^{-1}, if they are associated with the galaxy. The luminosities are similar to those of cataclysmic variables (which are interacting binaries containing a low-mass star transferring mass to a white dwarf) in their active state but are below the range for Galactic X-ray binaries in their bright X-ray states.

4.2. Carina dwarf galaxy

We applied a conversion in which 1 ct/ksec in the 0.2–10 keV band is equivalent to an unabsorbed flux of 1.6×10^{-14} erg cm^{-2} s^{-1} in the 0.1–10 keV band. If the sources are in Car, they would have luminosities $\sim 3 \times 10^{34}$–1×10^{36} erg s^{-1}. These luminosities are higher than those of cataclysmic variables but are comparable with those of X-ray binaries powered by wind-fed accretion (cf. sources in Table A of Muno et al. 2003).

5. X-ray colours

5.1. Sagittarius dwarf galaxy

Figure 2 shows the colour-colour plots of the sources in the Sgr field. We considered the colours $x \equiv (H - M)/(H + M + S)$ and $y \equiv (M - S)/(H + M + S)$ following the convention of Prestwich et al. (2003), Soria & Wu (2003) and Swartz et al. (2004) that S, M and H corresponding to count rates in the 0.3–1, 1–2 and 2–8 keV bands. We compared the colours of the sources with 4 spectral models: a blackbody model ($kT_{\rm bb} = 0.1$ keV), a disk blackbody model ($kT_{\rm dbb} = 0.5$ and 1 keV), an optically thin thermal plasma model ($kT_{\rm th} = 0.5$ keV) and a power-law model ($\Gamma = 1.4$ and 2.0). In each model, we considered a range of absorption column densities ranging from the line-of-sight Galactic absorption ($N_{\rm H} = 1.2 \times 10^{21}$ cm^{-2}) to a hydrogen column density of $N_{\rm H} = 5 \times 10^{22}$ cm^{-2}. The colour tracks of the models generally start at low y-colour values and then increase with absorption. Except for the very soft spectral models (e.g. blackbody with $kT_{\rm bb} = 0.1$ keV) the x-colour value increases with absorption. For sufficiently large absorption the colour tracks of the hard models (e.g. power law models, regardless of the photon index) converge. The soft models with different parameters, however, follow separate tracks.

The majority of the sources in the Sgr field have colours consistent with those of the absorbed power law or absorbed disk blackbody spectra, although some sources may require combined blackbody and power-law spectra to explain their colours. These spectra are typical of AGN and Galactic X-ray binaries, but we can single out the few stellar candidates from the background sources easily based on this set of X-ray data alone.

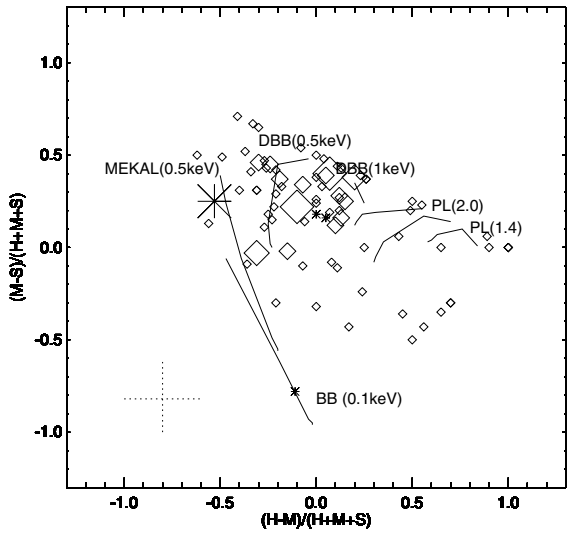

Fig. 2. The colour-colour plot for the sources in the Sgr field. S, M and H correspond to photon count rates in the 0.3–1, 1–2 and 2–8 keV bands. The size of the symbol indicates the number of photon counts in the 0.3–8 keV band. The solid lines show the predicted colour-colour track assuming different models: BB (Blackbody), MEKAL (optically thin plasma), DBB (disk blackbody), PL (power law). The temperature/slope of the model is shown in brackets. The absorption is assumed to start at the absorption to the edge of our Galaxy and then increases up to $N_{\rm H} = 5 \times 10^{22}$ cm^{-2}. In the lower corner we show the typical size of the errorbars for a moderately bright source (source number 31). Sources which had bright optical counterparts (and hence likely foreground stars) are shown as "stars".

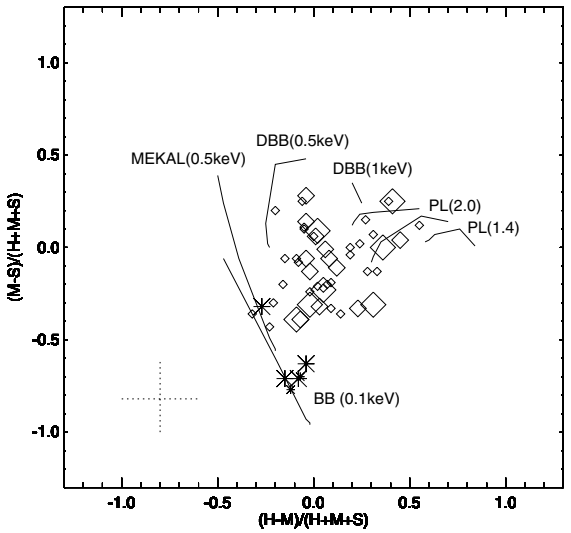

Fig. 3. As Figure 2 but for sources in the Car field. Otherwise S, M and H correspond to photon count rates in the 0.2–1, 1–2 and 2–10 keV bands. The size of the symbol indicates the number of photon counts in the 0.2–10 keV band. The absorption is assumed to start at the absorption to the edge of our Galaxy and then increases up to $N_{\rm H} = 1 \times 10^{22}$ cm^{-2}. In the lower corner we show the typical size of the errorbars for a moderately bright source (source number 23).

We note that some of the Sgr sources (No. 6, 9, 30, 46, 57 and 69 in Tables A) have very soft spectra. They lie close to the tracks of the blackbody ($kT_{\rm bb} = 0.1$ keV) model and the optically thin thermal ($kT_{\rm th} = 0.5$ keV) model. Their colours are not consistent with AGN X-ray spectra, which would lie closer to the harder colour-colour tracks.

5.2. Carina dwarf galaxy

Figure 3 shows the colours of the Car sources in the (H–M)/(H+M+S), (M–S)/(H+M+S) plane. Here S, M and H represent the 0.2–1, 1–2 and 2–10 keV bands. The colours for various spectral models with absorption column densities starting from the column density to the edge of the Galaxy (3.9×10^{20} cm^{-2}) to the column density of 1×10^{22} cm^{-2} are also shown for comparison. Despite the different detectors and slightly different energy bands used, the model tracks are similar to those in the colour-colour plot of the Sgr case. The sources have a wide spread in colour, as expected for background AGN with different absorption column density. There are roughly 3 sources which lie close to the tracks of the blackbody model ($kT_{\rm bb} = 0.1$ keV) and optically thin thermal plasma model ($kT_{\rm th} = 0.5$ keV). They are sources No. 17, 25 and 30 as listed in Table A.2. The colours of these sources are not consistent with AGN, and they are likely to be foreground stellar sources or sources inside the Car dSph.

6. Discussion & conclusions

We have performed X-ray observations of the Sgr and Car fields. Our observations reached a sensitivity limit (unabsorbed) $\sim 1 \times 10^{32}$ erg s^{-1} for the Sgr field and 3×10^{34} erg s^{-1} for the Car field. We have identified a total of 80 sources (in the 0.3–8 keV energy band) in the Sgr field (excluding the 7 sources which we have identified as being in the globular cluster M 54) and 53 sources (in the 0.2–10 keV band) in the Car field. At energies >2 keV we found 42 sources in the Sgr field and 40 in the Car field (these numbers do not include objects which are likely to be foreground stars). Based on the CDF-S we estimate that 55–79 background AGN would be in the Sgr field and 16–34 in the Car field. (The expected numbers will vary to some extent since the number of AGN varies from field to field.) The source numbers in the two field are broadly consistent with the expected number of background AGN. However, from the analysis of X-ray colours, we have found a small number of sources which have colours which are difficult to be explained by spectral models appropriates for AGN. We therefore propose that these are candidate stellar X-ray sources. The nature of these sources may be determined by follow-up X-ray observations or by identifying their optical/IR counterparts. Both Sgr and Car have low galactic latitudes ($b = -14°$ and $-22°$ respectively), which gives rise to a number of possible optical counterparts for many of the X-ray sources. The search for the optical counterparts to the X-ray sources will be discuss in detail in a future paper.

We note that Maccarone et al. (2005) found a small number of X-ray sources which are believed to belong to the Sculptor (Scu) dSph. These sources have X-ray luminosities $L_{\rm X} = 6$–90×10^{33} erg s^{-1}. The optical counterparts of these sources are relatively easy to identify as Scu has a high galactic latitude ($b = -83°$). The interstellar absorption to the edge of the Galaxy towards the direction of Car and Scu are similar (3.9×10^{20} cm^{-2} and 2.0×10^{20} cm^{-2} respectively). If we take a naive view that the number of X-ray sources are proportional to total stellar mass of the host galaxy, then we may obtain an estimate of the number of sources to be detected in Car from the results of Scu (we acknowledge that the reality is likely to be more complex since they have different star formation histories).

The Scu dSph has a core radius of 5.8′ and the field of view of the *Chandra* observations of Scu covered an area of $\sim 17' \times 17'$. The observations therefore covered a large fraction

of the galaxies mass ($6.4 \times 10^6\ M_\odot$). The field of view of the *XMM-Newton* observations of Car were much larger than the core radius of 8.8′ and covered a large fraction of the galaxies mass ($1.3 \times 10^7\ M_\odot$). (These parameters are taken from Mateo 1998). The *XMM-Newton* observations of Car were sensitive to X-ray luminosities $>3 \times 10^{34}$ erg s^{-1}: there were 2 Scu sources with luminosities greater than this. If we assume that the number of X-ray sources scales with the total stellar mass of the galaxy there will be roughly 2 sources with $L_X > 3 \times 10^{34}$ erg s^{-1} in Car. This suggests that some of the 3 soft X-ray sources in the Car field could actually be located in the Car dSph.

We observed only a small fraction of the sky coverage of the Sgr dSph – roughly 0.05%. The total mass of the Sgr dSph is $\sim 10^9\ M_\odot$ (Ibata et al. 1995), but we sampled a fraction of the galaxy with a total mass of $\sim 5 \times 10^5\ M_\odot$. If we scale the number of X-ray sources with mass, 1 X-ray source in Sgr would imply a total number 4×10^5 of X-ray sources with $L_X > 10^{32}$ erg s^{-1} in the Milky Way. This number is obviously rather uncertain for various reasons, and what fraction of these sources can be detected in a snap-shot is unclear given that a substantial fraction of the sources are transients or variable sources.

Birth-death models (e.g. Wu 2001) predict a primordial X-ray source population in all galaxies. These sources are remnants of the first generation stars formed with the galaxy. Suppose that the slope of the luminosity function of these source is similar to the faint end of the luminosity function of the bright bulge sources in M 81 (see Tennant et al. 2001), we would set an upper limit that fewer than 100 primordial X-ray sources with luminosity exceeding $\sim 10^{36}$ erg s^{-1} are in large spiral galaxies similar to M 81 or the Milky Way. However, the luminosity function of the primordial X-ray sources would show an exponential cut-off (a consequence of aging effects), beyond which the source counts drop rapidly. The number of primordial sources with such luminosities should in fact be much fewer since fainter sources can survive for a long time. Our observation of Sgr was sensitive down to $L_X \sim 1 \times 10^{32}$ erg s^{-1}, which is sufficient to detect most of the persistent bright X-ray binaries and moderately bright CVs. If the soft sources which we found belong to the host dSph, then they may be candidate primordial X-ray sources.

Acknowledgements. This is work based on observations obtained with *XMM-Newton*, an ESA science mission with instruments and contributions directly funded by ESA Member States and the USA (NASA). We thank Joe DePasquale for help in scheduling the *Chandra* observations. KW acknowledges the support for his visits to the University of Sydney through an Australian NSW State Expatriate Researcher Award. We thank the anonymous referee for useful comments and suggestions.

References

Cannon, R. D., Hawarden, T. G., & Tritton, S. B. 1977, MNRAS, 180, 81
Fabbiano, G. 2003, ChJAA, 3, Suppl., 193
Gizis, J. E., Mould J. R., & Djorgovski, S. 1993, PASP, 105, 871
Hurley-Keller, D., Mateo, M., & Nemec, J. 1998, AJ, 115, 1840
Ibata, R. A., Gilmore, G., & Irwin M. J. 1994, Nature, 370, 194
Ibata, R. A., Gilmore, G., & Irwin M. J. 1995, MNRAS, 277, 781
Kong, A. K. H., DiStefano, R., Garcia, M. R., & Greiner, J. 2003, ApJ, 585, 293
Layden, A. C., & Sarajedini, A. 2000, AJ, 119, 1760
Maccarone, T. J., Kundu, A., Zepf, S. E., Piro, A. L., & Bildsten, L. 2005, MNRAS, 364, L61
Mateo, M. 1998, ARA&A, 36, 435
Marzke, R. O., & da Costa, L. N. 1997, AJ, 113, 185
Muno, M. P., Baganoff, F. K., Bautz, M. W., et al. 2003, ApJ, 589, 225
Prestwich, A., Irwin, J. A., Kilgard, R. E., et al. 2003, ApJ, 595, 719
Ramsay, G., & Wu, K. 2006, A&A, 447, 199
Rosati, P., Tozzi, P., Giacconi, R., et al. 2002, ApJ, 566, 667
Soria, R., & Wu, K. 2003, A&A, 410, 56
Strüder, L., Briel, U., Dennerl, K., et al. 2001, A&A, 365, L18
Swartz, D. A., Ghosh, K. K., McCollough, M. L., et al. 2003, ApJS, 144, 213
Swartz, D. A., Ghosh, K. K., Tennant, A. F., & Wu, K. 2004, ApJS, 154, 519
Tennant, A. F., Wu, K., Ghosh, K. K., Kolodziejczak, J. J., & Swartz, D. A. 2001, ApJ, 549, L43
Turner, M., Abbey, A., Arnaud, M., et al. 2001, A&A, 365, L27
Wheatland, M. S. 2004, ApJ, 609, 1134
Wu, K. 2001, PASA, 18, 443
van den Bergh, S. 2000, The Galaxies of the local group, Cambridge, CUP
Zacharias, N., Urban, S. E., Zacharias, M. I., et al. 2004, AJ, 127, 3043
Zang, Z., & Meurs, E. J. A. 2001, ApJ, 556, 24

Online Material

Appendix A: Source lists

Table A.1. The X-ray sources found in the *Chandra* observations of the Sgr field. We show the count rate (per 10 ks) found for each source in 4 energy bands and the hardness ratios, where *HR*1 = (H–M)/(H+M+S) and *HR*2 = (M–S)/(H+M+S), where H is the counts in the 2–8 keV band, M the counts in the 1–2 keV band and S the counts in the 0.3–1 keV band. In the final column we show the magnitude (close to the *R* band for that source in the UCAC2 catalogue).

Src	RA	Dec	0.3–8 keV		0.3–1 keV		1–2 keV		2–8 keV		*HR*1		*HR*2		UCAC2
	(2000)			±		±		±		±		±		±	mag
1	18 54 26.24	–30 29 40.3	12.1	2.0	1.3	0.7	4.7	1.2	6.1	1.4	0.12	0.17	0.28	0.20	
2	18 54 26.50	–30 34 24.3	2.7	0.9	0.3	0.3	1.0	0.6	1.3	0.7	0.12	0.36	0.27	0.31	
3	18 54 26.67	–30 27 08.1	3.0	1.0	0.3	0.3	1.3	0.7	1.4	0.7	0.03	0.33	0.33	0.32	
4	18 54 27.43	–30 31 52.9	1.0	0.6	0.0	0.0	0.0	0.0	1.0	0.6	1.00	1.16	0.00	0.00	
5	18 54 28.14	–30 33 30.7	1.7	0.7	0.3	0.3	0.7	0.5	0.7	0.5	0.00	0.00	0.24	0.37	
6	18 54 33.14	–30 31 21.5	3.4	1.1	2.0	0.8	1.0	0.6	0.3	0.3	–0.21	0.24	–0.30	0.36	
7	18 54 33.32	–30 27 49.9	7.7	1.6	2.0	0.8	4.4	1.2	1.3	0.7	–0.40	0.30	0.31	0.26	
8	18 54 34.05	–30 25 06.3	10.8	1.9	2.0	0.8	3.7	1.1	5.1	1.3	0.13	0.18	0.16	0.16	
9	18 54 35.25	–30 26 29.3	4.0	1.2	0.7	0.5	2.7	0.9	0.7	0.5	–0.49	0.39	0.49	0.39	
10	18 54 35.38	–30 31 28.1	3.4	1.1	0.7	0.5	1.7	0.7	1.0	0.6	–0.21	0.30	0.29	0.31	
11	18 54 36.00	–30 25 10.4	8.1	1.6	1.0	0.6	4.4	1.2	2.7	0.9	–0.21	0.22	0.42	0.30	
12	18 54 36.40	–30 27 27.9	1.0	0.6	0.3	0.3	0.0	0.0	0.7	0.5	0.70	0.71	–0.30	0.37	
13	18 54 36.41	–30 27 40.7	3.7	1.1	1.3	0.7	1.7	0.7	0.7	0.5	–0.27	0.28	0.11	0.27	
14	18 54 37.35	–30 34 23.8	2.7	0.9	1.0	0.6	0.7	0.5	1.0	0.6	0.11	0.30	–0.11	0.30	
15	18 54 37.66	–30 32 25.7	5.1	1.3	1.3	0.7	2.0	0.8	1.7	0.7	–0.06	0.22	0.14	0.23	
16	18 54 38.93	–30 31 29.3	4.0	1.2	0.7	0.5	2.4	0.9	1.0	0.6	–0.34	0.33	0.41	0.35	
17	18 54 39.08	–30 26 08.7	8.4	1.7	0.3	0.3	2.0	0.8	6.1	1.4	0.49	0.37	0.20	0.17	
18	18 54 40.17	–30 27 01.6	3.0	1.0	1.7	0.7	0.7	0.5	0.7	0.5	0.00	0.00	–0.32	0.34	
19	18 54 40.59	–30 32 47.7	1.7	0.7	0.7	0.5	0.3	0.3	0.7	0.5	0.24	0.37	–0.24	0.37	
20	18 54 41.54	–30 27 44.4	4.0	1.2	1.7	0.7	1.3	0.7	1.0	0.6	–0.07	0.23	–0.10	0.25	
21	18 54 42.13	–30 36 51.1	4.7	1.2	2.0	0.8	0.3	0.3	2.4	0.9	0.45	0.34	–0.36	0.29	
22	18 54 43.00	–30 34 11.6	1.3	0.7	0.3	0.3	0.7	0.5	0.3	0.3	–0.31	0.48	0.31	0.48	
23	18 54 43.67	–30 26 35.4	6.4	1.5	0.7	0.5	3.7	1.1	2.0	0.8	–0.27	0.27	0.47	0.34	
24	18 54 43.89	–30 29 40.4	2.4	0.9	1.0	0.6	0.0	0.0	1.3	0.7	0.56	0.50	–0.43	0.40	
25	18 54 44.49	–30 25 09.5	4.0	1.2	1.0	0.6	1.0	0.6	2.0	0.8	0.25	0.29	0.00	0.00	
26	18 54 45.51	–30 25 11.3	10.4	1.9	1.3	0.7	6.1	1.4	3.0	1.0	–0.30	0.24	0.46	0.31	
27	18 54 47.01	–30 26 58.2	2.7	0.9	0.0	0.0	1.0	0.6	1.7	0.7	0.26	0.39	0.37	0.34	
28	18 54 49.04	–30 23 32.3	0.7	0.5	0.3	0.3	0.0	0.0	0.3	0.3	0.50	0.61	–0.50	0.61	
29	18 54 49.07	–30 23 55.8	3.7	1.1	0.0	0.0	2.0	0.8	1.7	0.7	–0.08	0.29	0.54	0.44	
30	18 54 49.13	–30 25 51.2	4.7	1.2	2.4	0.9	2.0	0.8	0.3	0.3	–0.36	0.29	–0.09	0.26	
31	18 54 49.22	–30 25 02.0	39.1	3.6	13.5	2.1	23.2	2.8	2.4	0.9	–0.53	0.34	0.25	0.18	13.6
32	18 54 49.38	–30 31 05.6	4.7	1.2	0.7	0.5	1.0	0.6	3.0	1.0	0.43	0.36	0.06	0.17	
33	18 54 49.88	–30 31 38.6	2.4	0.9	0.3	0.3	1.3	0.7	0.7	0.5	–0.26	0.41	0.43	0.42	
34	18 54 52.97	–30 35 41.8	3.7	1.1	0.3	0.3	1.7	0.7	1.7	0.7	0.00	0.00	0.38	0.31	
35	18 54 54.08	–30 25 40.1	3.0	1.0	0.0	0.0	0.7	0.5	2.4	0.9	0.55	0.52	0.23	0.23	
36	18 54 54.60	–30 30 42.9	4.4	1.2	0.0	0.0	1.7	0.7	2.7	0.9	0.23	0.31	0.39	0.32	
37	18 54 54.72	–30 26 55.2	2.7	0.9	0.3	0.3	0.3	0.3	2.0	0.8	0.65	0.54	0.00	0.00	
38	18 54 54.90	–30 31 25.4	11.1	1.9	1.3	0.7	4.0	1.2	5.7	1.4	0.15	0.19	0.25	0.19	
39	18 54 56.41	–30 35 08.4	2.7	0.9	2.4	0.9	0.3	0.3	0.0	0.0	–0.11	0.14	–0.78	0.71	13.0
40	18 54 57.28	–30 32 38.1	6.1	1.4	0.0	0.0	2.7	0.9	3.4	1.1	0.11	0.25	0.44	0.35	

Table A.1. continued.

Src	RA	Dec	0.3–8 keV		0.3–1 keV		1–2 keV		2–8keV		*HR*1		*HR*2		UCAC2
	(2000)			±		±		±		±		±		±	mag
41	18 54 57.37	–30 22 19.9	2.0	0.8	0.0	0.0	1.3	0.7	0.7	0.5	–0.30	0.48	0.65	0.58	
42	18 54 59.39	–30 23 51.6	3.4	1.1	0.0	0.0	2.4	0.9	1.0	0.6	–0.41	0.43	0.71	0.57	
43	18 55 00.13	–30 30 49.5	17.5	2.4	2.7	0.9	9.1	1.8	5.7	1.4	–0.19	0.17	0.37	0.25	
44	18 55 04.56	–30 26 32.5	17.8	2.5	7.1	1.5	6.7	1.5	4.0	1.2	–0.15	0.14	–0.02	0.12	
45	18 55 05.33	–30 31 06.2	2.7	0.9	0.7	0.5	1.3	0.7	0.7	0.5	–0.22	0.34	0.22	0.34	
46	18 55 06.63	–30 31 27.3	2.4	0.9	1.0	0.6	1.3	0.7	0.0	0.0	–0.56	0.50	0.13	0.41	
47	18 55 06.88	–30 32 24.3	1.3	0.7	0.3	0.3	0.7	0.5	0.3	0.3	–0.31	0.48	0.31	0.48	
48	18 55 07.92	–30 25 31.7	4.0	1.2	0.0	0.0	1.0	0.6	3.0	1.0	0.50	0.47	0.25	0.24	
49	18 55 07.99	–30 26 20.8	3.0	1.0	0.0	0.0	1.3	0.7	1.7	0.7	0.13	0.34	0.43	0.38	
50	18 55 08.38	–30 30 00.3	3.4	1.1	0.0	0.0	1.7	0.7	1.7	0.7	0.00	0.00	0.50	0.41	
51	18 55 10.67	–30 26 51.1	44.4	3.9	9.8	1.8	19.5	2.6	15.2	2.3	–0.10	0.10	0.22	0.15	
52	18 55 10.72	–30 22 14.1	9.8	1.8	0.0	0.0	4.7	1.2	5.1	1.3	0.04	0.18	0.48	0.36	
53	18 55 10.79	–30 31 25.6	1.0	0.6	0.3	0.3	0.0	0.0	0.7	0.5	0.70	0.71	–0.30	0.37	
54	18 55 10.90	–30 21 18.4	3.0	1.0	0.0	0.0	0.0	0.0	3.0	1.0	1.00	1.05	0.00	0.00	
55	18 55 11.39	–30 20 52.4	12.8	2.1	0.7	0.5	5.7	1.4	6.4	1.5	0.05	0.16	0.39	0.27	
56	18 55 11.53	–30 26 19.7	3.0	1.0	0.0	0.0	2.0	0.8	1.0	0.6	–0.33	0.41	0.67	0.55	
57	18 55 14.73	–30 35 41.6	20.5	2.6	9.4	1.8	8.8	1.7	2.4	0.9	–0.31	0.21	–0.03	0.12	
58	18 55 15.48	–30 28 09.2	23.2	2.8	0.3	0.3	9.1	1.8	13.8	2.2	0.20	0.18	0.38	0.26	
59	18 55 16.15	–30 28 58.8	4.0	1.2	0.7	0.5	2.0	0.8	1.3	0.7	–0.18	0.28	0.33	0.30	
60	18 55 16.79	–30 31 44.6	5.4	1.3	1.0	0.6	2.0	0.8	2.4	0.9	0.07	0.23	0.19	0.21	
61	18 55 18.42	–30 33 33.7	5.4	1.3	0.0	0.0	0.3	0.3	5.1	1.3	0.89	0.78	0.06	0.07	
62	18 55 21.81	–30 27 12.8	8.1	1.6	1.7	0.7	3.0	1.0	3.4	1.1	0.05	0.19	0.16	0.18	13.6
63	18 55 21.92	–30 30 10.7	2.4	0.9	1.3	0.7	0.3	0.3	0.7	0.5	0.17	0.27	–0.43	0.42	
64	18 55 22.13	–30 32 13.1	8.8	1.7	2.7	0.9	4.0	1.2	2.0	0.8	–0.23	0.21	0.15	0.19	
65	18 55 22.67	–30 33 18.5	13.8	2.2	3.0	1.0	4.7	1.2	6.1	1.4	0.10	0.15	0.12	0.13	
66	18 55 24.19	–30 28 04.2	11.4	2.0	1.3	0.7	6.4	1.5	3.7	1.1	–0.24	0.22	0.45	0.31	
67	18 55 25.72	–30 27 17.0	2.7	0.9	0.0	0.0	1.0	0.6	1.7	0.7	0.26	0.39	0.37	0.34	
68	18 55 26.12	–30 26 29.0	8.4	1.7	1.3	0.7	3.0	1.0	4.0	1.2	0.12	0.20	0.20	0.19	
69	18 55 27.17	–30 26 34.1	3.4	1.1	0.7	0.5	2.4	0.9	0.3	0.3	–0.62	0.48	0.50	0.44	
70	18 55 27.57	–30 24 56.1	10.1	1.9	1.3	0.7	4.7	1.2	4.0	1.2	–0.07	0.17	0.34	0.24	
71	18 55 27.71	–30 29 25.5	9.1	1.8	0.3	0.3	0.3	0.3	8.4	1.7	0.90	0.71	0.00	0.00	
72	18 55 27.91	–30 25 12.0	3.7	1.1	1.3	0.7	1.0	0.6	1.3	0.7	0.08	0.26	–0.08	0.26	
73	18 55 29.27	–30 25 03.2	3.4	1.1	0.0	0.0	0.0	0.0	3.4	1.1	1.00	1.05	0.00	0.00	
74	18 55 29.79	–30 28 29.1	5.7	1.4	1.7	0.7	2.7	0.9	1.3	0.7	–0.25	0.25	0.18	0.22	
75	18 55 32.01	–30 34 07.8	2.7	0.9	0.3	0.3	1.7	0.7	0.7	0.5	–0.37	0.39	0.52	0.42	
76	18 55 32.64	–30 27 06.7	1.0	0.6	0.3	0.3	0.3	0.3	0.3	0.3	0.00	0.00	0.00	0.00	13.6
77	18 55 32.81	–30 32 58.9	6.1	1.4	1.3	0.7	2.4	0.9	2.4	0.9	0.00	0.00	0.18	0.21	15.4
78	18 55 33.91	–30 34 45.4	2.0	0.8	0.7	0.5	0.0	0.0	1.3	0.7	0.65	0.58	–0.35	0.35	
79	18 55 36.65	–30 29 00.2	8.1	1.6	1.3	0.7	3.4	1.1	3.4	1.1	0.00	0.00	0.26	0.22	
80	18 55 37.27	–30 30 36.7	119.5	6.3	5.4	1.3	52.9	4.2	61.3	4.5	0.07	0.07	0.40	0.25	

Table A.2. The X-ray sources in the Carina field as detected using sl XMM-Newton. We show the count rates in Cts/ksec in the 0.2–10 keV, 0.2–1 keV, 1–2 keV and 2–10 keV energy bands. The count rates refer to that detected in the EPIC MOS(1+2) detector, or the equivalent if detected only in the EPIC pn detector. We also show the hardness ratios, where *HR*1 = (H–M)/(H+M+S) and *HR*2 = (M–S)/(H+M+S), where H is the counts in the 2–10 keV band, M the counts in the 1–2 keV band and S the counts in the 0.2–1 keV band. In the final column we show the magnitude (close to the *R* band for that source in the UCAC2 catalogue).

Src	RA	Dec	0.2–10 keV		0.2–1 keV		1–2 keV		2–10 keV		*HR*1		*HR*2		UCAC2
	(2000)			±		±		±		±		±		±	mag
1	6 40 14.9	–50 58 23.1	4.2	0.8	0.6	0.3	1.2	0.3	2.3	0.6	0.27	0.23	0.15	0.14	
2	6 40 19.8	–50 58 23.0	34.9	1.7	38.6	1.8	14.5	1.1	8.7	1.2	–0.09	0.06	–0.39	0.23	
3	6 40 21.5	–51 00 56.7	8.0	1.0	2.3	0.5	2.8	0.4	2.9	0.6	0.01	0.09	0.06	0.09	
4	6 40 24.8	–51 06 16.6	5.2	1.1	0.9	0.4	1.1	0.4	3.6	0.9	0.45	0.33	0.04	0.10	
5	6 40 28.0	–50 59 17.6	9.2	1.0	8.3	0.9	2.6	0.4	6.6	1.0	0.23	0.15	–0.33	0.21	
6	6 40 28.6	–50 57 02.3	3.3	0.7	0.9	0.3	1.1	0.3	1.1	0.5	0.00	0.00	0.06	0.14	
7	6 40 34.1	–50 59 39.8	6.7	0.8	9.4	0.8	1.4	0.4	0.5	0.5	–0.08	0.07	–0.71	0.43	11.4
8	6 40 36.4	–50 53 18.5	4.6	0.7	1.2	0.3	1.7	0.4	1.5	0.5	–0.05	0.15	0.11	0.13	
9	6 40 36.4	–50 59 17.1	4.3	0.5	2.0	0.4	1.7	0.4	3.0	0.7	0.19	0.17	–0.04	0.09	
10	6 40 36.7	–50 49 20.7	3.5	0.9	0.6	0.3	1.4	0.4	1.2	0.6	–0.06	0.23	0.25	0.22	
11	6 40 41.2	–50 47 49.7	4.8	0.9	2.3	0.4	1.4	0.4	0.7	0.6	–0.16	0.19	–0.20	0.18	
12	6 40 44.7	–51 06 22.0	7.3	1.0	1.9	0.5	2.9	0.5	2.6	0.6	–0.04	0.11	0.14	0.12	
13	6 40 50.0	–50 56 31.8	2.8	0.4	2.4	0.4	0.9	0.3	1.3	0.6	0.09	0.15	–0.33	0.22	
14	6 40 53.6	–50 51 20.6	2.2	0.6	0.6	0.3	0.8	0.2	0.7	0.4	–0.05	0.21	0.10	0.18	
15	6 40 56.1	–50 52 32.6	2.6	0.5	6.1	0.7	0.8	0.3	0.0	0.2	–0.12	0.09	–0.77	0.52	12.2
16	6 40 59.2	–50 55 51.1	6.2	0.6	5.9	0.6	2.2	0.3	1.5	0.5	–0.07	0.07	–0.39	0.24	
17	6 41 00.2	–50 57 14.3	2.8	0.5	1.7	0.2	0.8	0.2	0.0	0.1	–0.32	0.21	–0.36	0.24	
18	6 41 00.6	–50 47 01.3	4.1	0.8	1.6	0.4	1.3	0.4	1.0	0.5	–0.08	0.17	–0.08	0.15	
19	6 41 04.6	–51 00 00.0	7.7	0.6	12.7	0.8	2.3	0.3	1.6	0.5	–0.04	0.04	–0.63	0.39	15.4
20	6 41 06.9	–50 47 40.8	3.1	0.7	3.1	0.6	1.7	0.5	2.2	0.9	0.07	0.15	–0.20	0.16	
21	6 41 07.5	–51 07 05.5	4.4	0.8	2.9	0.5	4.0	0.6	8.9	1.2	0.31	0.21	0.07	0.07	
22	6 41 09.1	–51 02 06.7	3.8	0.5	3.6	0.5	1.9	0.3	2.3	0.6	0.05	0.09	–0.22	0.15	
23	6 41 09.6	–51 09 07.8	12.2	1.2	9.0	1.0	2.6	0.5	9.1	1.4	0.31	0.21	–0.31	0.20	
24	6 41 12.3	–50 54 20.3	3.0	0.5	2.6	0.4	2.2	0.3	1.6	0.5	–0.09	0.11	–0.06	0.09	
25	6 41 18.9	–50 54 48.8	2.2	0.4	2.6	0.4	1.3	0.2	0.4	0.4	–0.21	0.16	–0.30	0.21	
26	6 41 22.1	–51 04 11.7	5.0	0.6	0.8	0.2	2.2	0.3	2.0	0.4	–0.04	0.10	0.28	0.18	
27	6 41 23.9	–50 47 58.7	5.6	0.8	4.1	0.6	3.5	0.5	3.1	0.8	–0.04	0.09	–0.06	0.08	
28	6 41 28.6	–51 00 58.0	2.9	0.4	0.1	0.1	0.8	0.2	1.9	0.3	0.39	0.28	0.25	0.18	
29	6 41 30.8	–50 56 59.1	4.8	0.5	9.5	0.7	1.4	0.3	0.6	0.4	–0.07	0.06	–0.70	0.44	12.1
30	6 41 33.0	–50 59 34.1	2.1	0.4	2.1	0.3	0.8	0.2	0.1	0.3	–0.23	0.18	–0.43	0.28	
31	6 41 34.5	–50 48 24.9	7.8	0.6	4.1	0.6	3.4	0.5	4.4	0.8	0.08	0.09	–0.06	0.07	
32	6 41 37.7	–50 56 47.7	3.7	0.5	1.4	0.2	1.2	0.2	0.7	0.3	–0.15	0.14	–0.06	0.09	
33	6 41 40.3	–51 00 05.4	7.5	0.6	6.4	0.5	1.1	0.2	0.0	0.1	–0.15	0.10	–0.71	0.49	9.2
34	6 41 40.7	–51 04 47.1	2.1	0.4	1.9	0.4	0.6	0.3	1.1	0.6	0.14	0.20	–0.36	0.26	
35	6 41 44.3	–50 51 54.0	2.5	0.5	2.0	0.4	2.0	0.4	3.4	0.6	0.19	0.15	0.00	0.00	
36	6 41 46.1	–50 50 22.9	65.8	3.9	68.5	1.9	29.6	1.2	26.9	1.4	–0.02	0.02	–0.31	0.18	
37	6 41 46.4	–50 48 03.0	4.8	0.7	2.3	0.4	1.2	0.3	1.1	0.4	–0.02	0.11	–0.24	0.18	
38	6 41 48.0	–50 49 40.3	4.9	0.8	4.3	0.6	2.5	0.4	7.0	0.9	0.33	0.21	–0.13	0.09	
39	6 41 48.3	–51 13 43.2	37.6	1.7	2.3	0.9	22.1	1.8	53.9	3.4	0.41	0.27	0.25	0.17	
40	6 41 48.9	–50 59 41.9	1.6	0.4	0.4	0.2	0.7	0.2	0.4	0.2	–0.20	0.22	0.20	0.22	
41	6 41 49.2	–50 47 11.5	10.1	1.0	5.0	0.7	4.9	0.6	13.2	1.4	0.36	0.23	0.00	0.04	
42	6 41 49.2	–51 06 51.2	3.1	0.7	0.5	0.4	1.4	0.4	5.4	1.0	0.55	0.38	0.12	0.11	
43	6 41 51.5	–50 57 14.9	9.5	0.7	11.0	0.7	4.4	0.5	5.0	0.6	0.03	0.04	–0.32	0.19	
44	6 41 51.6	–50 46 38.6	3.5	0.7	5.0	0.7	3.0	0.5	7.2	1.1	0.28	0.19	–0.13	0.10	
45	6 41 59.5	–51 09 46.8	5.8	1.1	2.8	0.6	1.4	0.4	0.2	0.4	–0.27	0.21	–0.32	0.25	16.2
46	6 42 00.2	–51 00 29.0	5.6	0.6	4.5	0.5	3.1	0.4	2.9	0.6	–0.02	0.07	–0.13	0.10	
47	6 42 05.3	–51 03 44.8	2.4	0.6	2.0	0.4	1.1	0.4	1.2	0.7	0.02	0.19	–0.21	0.18	
48	6 42 05.8	–51 07 47.4	6.4	1.0	4.4	0.8	3.1	0.6	4.6	1.1	0.12	0.13	–0.11	0.10	
49	6 42 09.4	–51 02 51.6	4.3	0.7	1.0	0.3	1.1	0.3	2.1	0.4	0.24	0.18	0.02	0.10	
50	6 42 11.9	–50 53 37.6	8.2	0.8	2.6	0.3	2.5	0.3	3.0	0.5	0.06	0.08	–0.01	0.05	
51	6 42 17.4	–51 01 44.4	10.9	0.9	2.8	0.4	3.8	0.5	4.0	0.6	0.02	0.07	0.09	0.08	
52	6 42 25.0	–50 59 52.3	5.0	0.6	4.3	0.6	2.4	0.4	3.3	0.8	0.09	0.10	–0.19	0.13	
53	6 42 47.4	–51 00 25.7	21.5	1.7	15.4	1.4	7.9	1.0	9.7	1.5	0.05	0.06	–0.23	0.14	